Metal Ion Complexation: A Route to 2D Templates?

Steven De Feyter,*[a] Mohamed M. S. Abdel-Mottaleb,[a, c] Norbert Schuurmans,[b] Bas J. V. Verkuijl,[b] Jan H. van Esch,*[b] Ben L. Feringa,[b] and Frans C. De Schryver[a]

Abstract: The two-dimensional ordering of a number of 2,2′-bipyridine derivatives at the liquid/solid interface has been investigated by scanning tunneling microscopy. By appropriate functionalization of the bipyridine units, their intermolecular distance can be tuned, which has proved to be crucial for complexation with metal ions. The in situ addition of metal salts (Pd^{2+}, Cu^{2+}), leading to the formation of metal-bipyridine complexes, has a dramatic influence on the two-dimensional ordering of the molecules and suggests that these complexes could be used as templates.

Keywords: bipyridines · coordination · physisorption · scanning probe microscopySTM · self-assembly

Introduction

Due to the continuing need for miniaturization in electronics, the field of "nano"-electronics and surface "nano"-patterning has received considerable attention lately. Despite the extraordinary success of current techniques for microfabrication, new and alternative techniques are highly desirable. To comply with the demands set by the reduced size of the functional parts, it is of importance to control the ordering of the "components" on a surface. Several approaches exist, of which the so-called top-down approaches are the most popular, involving photolithography, electron beam lithography,[1] and "soft lithography".[2] In a top-down type approach, the sharp tip of an STM or an atomic force microscope (AFM) can be used in several lithography modes to form patterns on the nanoscale.[3–14]

As a bottom-up alternative, self-assembly — the spontaneous organization of molecules into stable, structurally well-defined aggregates — has been put forward as a possible paradigm for generating nanoscale templates under ambient conditions.[15–22] Although the principles of self-assembly apply to both physisorbed and chemisorbed monolayers, the latter approach has been most extensively applied for decorating surfaces, leading to patterns in which molecules such as alkane derivatives stand almost upright.[23] Tailoring the chemical composition along the alkyl chain allows the patterning of organic monolayers on the nanometer scale,[24] and this has also been shown for systems at the liquid/air interface, where the molecules lie with their long axes parallel to the substrate.[25,26] Self-assembly has also been used to directly form a nanotemplate that does not require further manipulation by an SPM probe. Based on metal complexation, examples have been reported of the formation of well-defined coordination arrays on surfaces (metallo-grids), which were found to possess interesting electronic, magnetic, and structural properties.[27,28] These coordination arrays were based on the self-assembly of nitrogen-containing ligands and a suitable metal ion.[29–31] Furthermore, by varying the molecular structure of the complex, a variation in the molecular orientation was observed. These experiments also show the possibility of building locally addressable storage devices for molecular electronics. Other examples include the self-assembly of metal-organic coordination complexes and networks.[32–35]

Our research is directed towards the development of new approaches for decorating surfaces at the supramolecular level,[36–38] and to use these patterns for the spatial organization of functional groups, such as addressable groups, catalytically active groups, and so on. The rigidity and directionality of the metal coordination mode of bipyridines make them among the most ubiquitous constituents of supra-

[a] Dr. S. De Feyter, Dr. M. M. S. Abdel-Mottaleb, Prof. F. C. De Schryver
Katholieke Universiteit Leuven, Department of Chemistry
Celestijnenlaan 200 F, 3001 Leuven (Belgium)
Fax: (+32) 16327989
E-mail: Steven.DeFeyter@chem.kuleuven.ac.be

[b] Dr. N. Schuurmans, B. J. V. Verkuijl, Dr. J. H. van Esch, Prof. B. L. Feringa
University of Groningen, Material Science Center, Stratingh Institute, Laboratory of Organic and Molecular Inorganic Molecular Chemistry, Nijenborg 4, 9747 AG Groningen, (The Netherlands)
E-mail: J.van.Esch@chem.rug.nl

[c] Dr. M. M. S. Abdel-Mottaleb
Current address: Abteilung Organische Chemie II der Universität Ulm, Albert-Einstein-Allee 11, 89081 Ulm (Germany)

DOI: 10.1002/chem.200305424

molecular assemblies.[39–43] Bipyridines have been widely used for the realization of discrete, highly ordered nanostructures based on transition metal coordination.[44] Based on their rich chemical properties we have chosen bipyridine-derived molecules as a basis for template formation, that is, the controlled 2D spatial disposition of metal centers that can act as anchor points for further functionalization.

Herein, we explore "in situ" the bipyridine unit as a complexation scaffold in physisorbed films at the liquid/solid and air/solid interfaces, and investigate the restructuring effect of adding metal salts to the adlayer. Previously, we have reported the complexation of palladium acetate with bipyridine units anchored on graphite, as visualized by scanning tunneling microscopy.[38] We have now extended the previous studies by investigating the effect of the intermolecular distance between the bipyridine units on their complexation properties at a surface. We have also considered symmetry-related effects, and have explored the complexation of different metal ions.

Results and Discussion

Two-dimensional patterns of bipyridine derivatives: Urea groups are a robust motif for the formation of extended ribbons of hydrogen-bonded molecules. Compounds containing two urea groups separated by a spacer are particularly interesting, since they can form up to eight hydrogen bonds with neighboring molecules.[45–49] From previous studies, it is clear that the intermolecular distance is often dictated by hydrogen bonding between the urea functionalities.[45–49] On the basis of these previous findings, it was anticipated that the aromatic moieties would not lie flat in relation to the substrate, but rather would be tilted due to the limited space available.[42] On the one hand, such an orientation could promote metal ion complexation at the liquid/solid interface, but on the other hand, the dominance of the hydrogen bonds might complicate the metal ion complexation. Motivated by these expectations and uncertainties, the 2D packing pattern of **1** (chemical structure: Scheme 1) at the liquid/solid interface was investigated. Upon applying a drop of a saturated solution of **1** in 1-phenyloctane or 1-octanol to the surface of graphite (HOPG), a well-ordered monolayer is spontaneously formed at the liquid/solid interface (Figure 1). The image is submolecularly resolved, which enables the identification of the different functionalities within the molecules. The molecules are ordered in rows, and the width of such a row (lamella) is indicated by ΔL_1. The bipyridine moieties appear as bright bands (black arrow) in the middle of the lamellae. They form an angle of $70 \pm 2°$ with respect to the lamella axis. The urea groups appear as two bright lines (small arrows) on either side of the bipyridine moiety. The alkyl chains are fully extended and form an angle of $81 \pm 1°$ with respect to the lamella axis. There is no indication of interdigitation. The intermolecular distance between two successive molecules within a lamella was found to be 4.6 ± 0.3 Å, which is in good agreement with the intermolecular distances found in other urea-containing systems[45–48] and is indicative of the formation of hydrogen bonds between the urea groups. Based on the packing parameters, a proposed model for the observed packing is depicted in Figure 1B. In this model, as expected, the intermolecular distance does not allow the bipyridine moieties to lie flat on the surface, and therefore a tilted arrangement is inferred. There is no information as to whether the nitrogen atoms of the pyridine moieties are oriented towards the graphite or the solution, nor on the eventual cisoid or transoid conformation adopted by the bipyridine.[50]

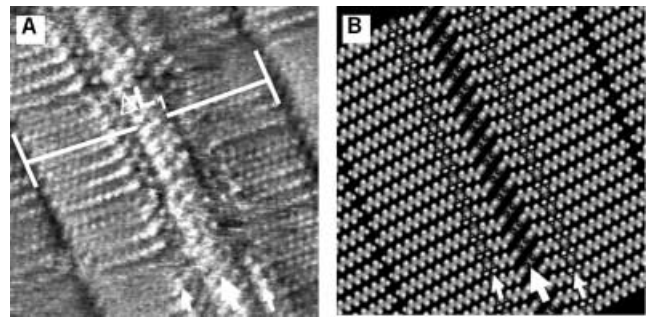

Figure 1. A) STM image of a monolayer composed of molecules of **1** at the liquid/solid interface. Bipyridine moieties appear as a bright tape in the middle of the lamella (big arrow), while the urea groups appear as two bright lines on either side of the bipyridine moieties (small arrows). ΔL_1 indicates a lamella. The image size is 10.8×10.8 nm^2; $I_{set} = 0.4$ nA, $V_{set} = -0.304$ V. B) A packing model for the monolayer observed in A). The bipyridine moieties are assumed to be tilted off the surface.

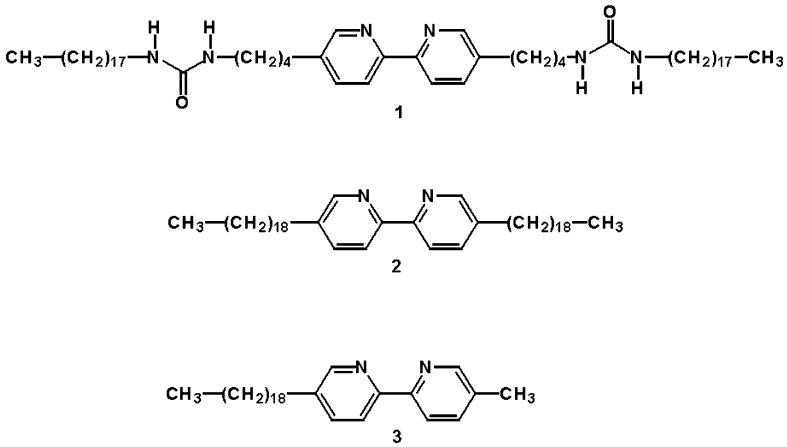

Scheme 1. Chemical structures of the bipyridine derivatives.

Urea-free bipyridine derivatives have also been investigated, the reason being that the absence of the urea groups puts less constraints on the intermolecular distance between adjacent bipyridine moieties, and thereby might affect the

metal ion complexation. Upon applying a drop of a solution of **2** in 1-phenyloctane to a graphite surface, a physisorbed monolayer is spontaneously formed at the liquid/solid interface.[38] Figure 2 shows an image of such a monolayer, as observed by STM. The image is submolecularly resolved, which enables us to identify the two aromatic rings of the bipyridine moiety (indicated by the two big arrows) as well as the aliphatic chains. The lamella is defined by two black troughs, which are characteristic for terminal methyl groups (indicated by the two small arrows). The bipyridine moieties form an angle of $64\pm2°$ while the aliphatic chains form an angle of $49\pm2°$, with respect to the lamella axis. For clarity, one molecular model of **2** has been superimposed on the STM image. Based on the contrast of the bipyridine moieties in the STM images it is obvious that all the molecules are equivalent along the lamella axis, and their chains appear to be fully extended. A molecular model of the observed packing is shown in Figure 2B. The distance between two neighboring molecules within a lamella measured along the lamella axis (a) is 6.9 ± 0.3 Å, and the distance between equivalent points in abutting lamellae ΔL_1 is 51.0 ± 1.6 Å. Note that the intermolecular distance is much larger (about a 50% increase) compared to that in the case of **1**. The packing parameters acquired from the STM image indicate that the bipyridine moieties are adsorbed parallel to the graphite plane, and that there is no interdigitation of the aliphatic chains from neighboring lamellae. Again, the data do not provide information on the conformation of the bipyridine units. In Figure 2B, a *cis* conformation has been arbitrarily assumed, as this conformation will allow metal complexation.

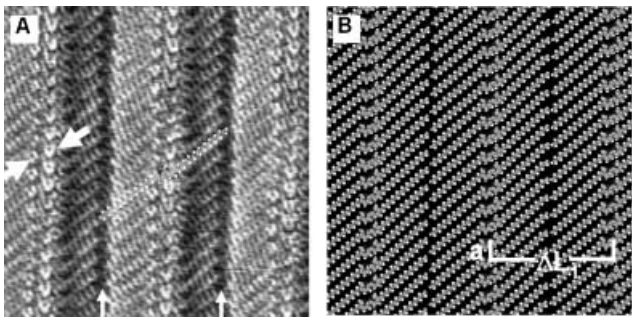

Figure 2. A) STM image of a monolayer of **2** physisorbed at the liquid/solid interface. Big arrows point to the aromatic rings of a bipyridine moiety; small arrows define the lamella boundaries. One molecular model is superimposed for clarity. The difference in contrast of the alkyl chains on either side of the bipyridine cores is due to a scanning artefact. The image area is 9.1×9.1 nm^2; $I_{set} = 1.2$ nA, $V_{set} = -0.244$ V. B) Molecular model of the monolayer, with $a = 6.9\pm0.3$ Å, $\Delta L_1 = 51.0\pm1.6$ Å. A *cis* conformation of the bipyridine units has been assumed arbitrarily.

In addition to the aforementioned highly uniform monolayers, some monolayers with packing irregularities were observed for **2** at the liquid/solid interface. Figure 3A and Figure 3B show lamellae of different widths. The small lamella shows the same packing pattern of **2** as observed in Figure 2A. In Figure 3A, two white arrows indicate what we believe to be the two pyridyl rings of the bipyridine moieties within a small lamella. The wider lamella ($\Delta L_2 = 59\pm1.5$ Å) consists of rows of two molecules of **2** stacked along the lamella direction. Instead of just two lines of bright structures, three bright lines are visible. Two molecular structures are superimposed on the image for clarity. In this case, the bipyridine moieties are supposed to lie head-to-head with one alkyl chain per bipyridine moiety adsorbed on the graphite surface while the other alkyl chain is thought to be dangling in the supernatant solution (in this tentative model, only one alkyl chain is shown). At present, we have no explanation for this counterintuitive observation and cannot rule out the possibility that the bipyridine unit may be partly tilted or even that part of the "visible" alkyl chain close to the bipyridine unit appears brighter because it is slightly lifted off the substrate. The width of the core in this case (18.2 ± 1.3 Å) is consistent with this assumption.

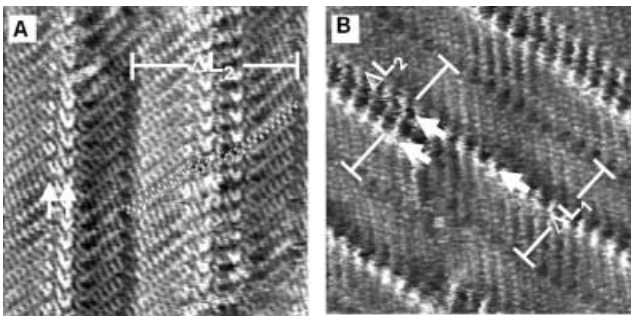

Figure 3. A) STM image of **2** showing two lamellae of different widths. Arrows indicate the rings of the bipyridine units. Two molecular structures are superimposed on the STM image for clarity. ΔL_2 indicates the width of the wider lamella. The image size is 9×9 nm^2; $I_{set} = 1.2$ nA, $V_{set} = -0.242$ V. B) STM image of **2** showing a change in the packing pattern within the same lamella. Single and double bipyridine moieties stacked along the lamella direction are indicated by big arrows. The image size is 10.6×10.6 nm^2; $I_{set} = 1.2$ nA, $V_{set} = -0.476$ V.

To investigate the origin of the packing irregularities observed in the monolayers of **2** and the effect of molecular symmetry on the 2D ordering, monolayer formation by **3**, bearing only one alkyl chain (see Scheme 1), was investigated at the liquid/solid interface. Figure 4 shows an STM image of the monolayer of **3** observed at the liquid/solid interface. The lamellar structure of the monolayer is evident. The bipyridine moieties appear as bright bands in the middle of the lamella and the alkyl chains appear as some-

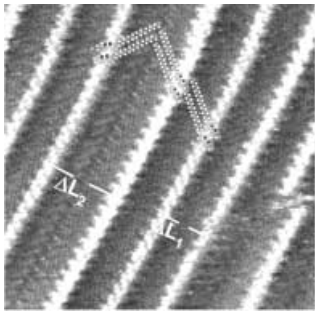

Figure 4. STM image of a monolayer of **3** at the liquid/solid interface. A lamellar structure is evident. The molecules are adsorbed in two different packing patterns, head-to-tail ($\Delta L_1 = 25.5\pm1.2$ Å) and tail-to-tail ($\Delta L_2 = 35.7\pm0.9$ Å). Six molecular structures are superimposed on the STM image. The image area is 15.2×15.2 nm^2; $I_{set} = 0.8$ nA, $V_{set} = -0.436$ V.

what darker than the bipyridine moieties. In this image, molecules adopt a head-to-tail packing as indicated by ΔL_1 (25.5 ± 1.2 Å) or a tail-to-tail packing as indicated by ΔL_2 (35.7 ± 0.9 Å). The intermolecular distance between neighboring molecules along a lamella axis is 6.5 ± 0.4 Å. The alkyl chains are not interdigitated.

In addition to the head-to-tail (ΔL_1) and tail-to-tail (ΔL_2) packings, double-core lamellae can be observed in the monolayer (Figure 5A: patterned arrows). In this case, the molecules are lying head-to-head. The core width is 16.7 ± 1.1 Å, which is in good agreement with the width of two bipyridine moieties, whereas the width of a single core is 8.6 ± 0.9 Å. Note that this core width (double core of **3**) is identical (within experimental error) to the double-core width in the case of monolayers of **2** at the liquid/solid interface. The intermolecular distance between neighboring molecules along the lamella is 6.8 ± 0.5 Å. Thus, there is no significant difference between lamellae with a head-to-head and those with a head-to-tail arrangement with respect to intermolecular distance. The alkyl chains are not interdigitated. In addition to the single-core and double-core lamellae observed for **3** at the liquid/solid interface, triple-core lamellae are also observed. Figure 5C shows a monolayer with such packing. A double-core lamella is indicated by the patterned arrows, while a triple-core lamella is indicated with black arrows. In the latter case, for the molecule adsorbed in the middle of the core, the alkyl chain will not be adsorbed on the surface. Thus, it is expected that the chain will be dangling in the supernatant solution. The width of the core (28.7 ± 1.5 Å) confirms the proposed packing. The predominant packing, however, is the head-to-tail mode. These data confirm the packing irregularities observed for **2** and indicate that they are intrinsic properties of alkylated bipyridines.

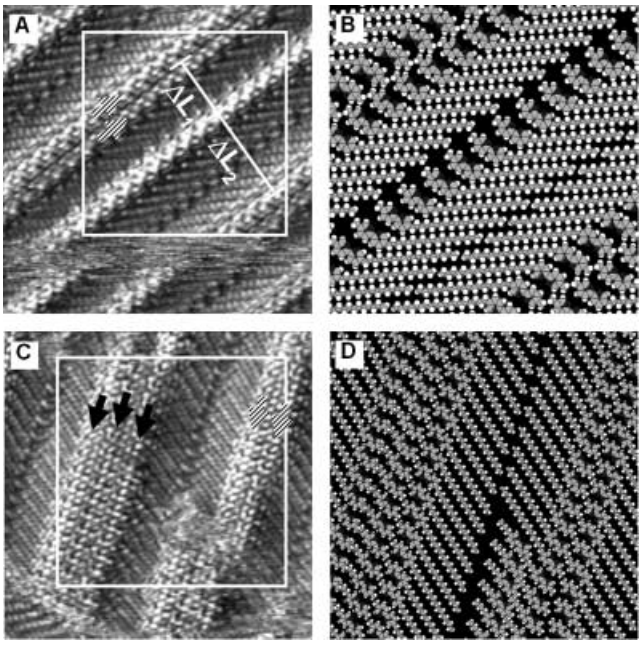

Figure 5. A) STM image of a monolayer of **3** at the liquid/solid interface. Head-to-tail (ΔL_1) and tail-to-tail (ΔL_2) packings are observed. Single-core and double-core lamellae are observed (patterned arrows). The image area is 11.5×11.5 nm^2; $I_{set} = 0.8$ nA, $V_{set} = -0.4$ V. B) Packing model of the area indicated in A). C) STM image of a monolayer of **3** at the liquid/solid interface. A double-core lamella (patterned arrows) and a triple-core lamella (black arrows) can be observed. The image area is 11.5×11.5 nm^2; $I_{set} = 0.8$ nA, $V_{set} = -0.5$ V. D) Packing model for the area indicated in C).

Complexation with metal ions: Once the two-dimensional ordering of the bipyridine derivatives was established, we proceeded to investigate their complexation with metal ions at the liquid/solid interface. A drop of a concentrated solution of the chosen metal ion was added in situ to the preformed bipyridine monolayer. In the case of **1**, in situ addition of complexed metal ions ($Pd(OAc)_2$, $PdCl_2$, $Cu(OAc)_2$, and $CuCl_2$) in 1-phenyloctane solutions did not result in any observable change in either the contrast or the packing pattern and parameters of the monolayers of **1**. Ex situ complexation of **1** did not result in the formation of a monolayer with different packing. Apparently, the close packing of the bipyridine moieties does not leave enough space for metal complexation to occur, and, most probably, the gain in free energy that would be achieved by metal complexation would not compensate for the loss of eight hydrogen bonds in the bipyridine-bis(urea) lamellae. Such a change in packing pattern would be necessary for the formation of the complex, and to allow for the accommodation of the metal atom within the monolayer. Another possibility might be the desorption of the complexed molecules from the surface.

After the successful imaging of monolayers of **2** at the 1-phenyloctane/graphite interface, a drop of a solution of $Pd(OAc)_2$ in 1-phenyloctane was applied. Within a couple of minutes, a spontaneous change in the monolayer packing pattern could be observed. Figure 6A shows an STM image of such a monolayer of **2** after the addition of $Pd(OAc)_2$. Two domains can be identified, domain A with a packing pattern similar to that previously observed for **2** (Figure 2A) and domain B with a new packing pattern, which is attributed to a bipyridine-metal complexed monolayer. In domain B, the core-to-core distance between abutting lamellae ($\Delta L_2 = 35.1 \pm 1.3$ Å) is smaller than that previously observed for **2** ($\Delta L_1 = 51.0 \pm 1.6$ Å). At the domain boundary, increased mobility of the molecules in some locations is evident (arrows). Figure 6B shows a large-scale image of the different domains observed after the addition of $Pd(OAc)_2$. Domains A, B, C, and D are assigned to the uncomplexed monolayer, while domain E corresponds to a complexed monolayer. It should be noted that the co-existence of complexed and uncomplexed domains is only observed immediately after the addition of the complexing agent $Pd(OAc)_2$. In time, only monolayers with a packing pattern similar to that of domain B in Figure 6A (or domain E in Figure 6B) are observed. After the addition of the complexing agent, no packing irregularities were observed in the monolayer.

Figure 6C shows an STM image of the monolayer with the new packing pattern. The image is submolecularly resolved, which again enables us to identify the aliphatic chains as well as the complexation sites. The bipyridine moieties cannot be discerned; instead, well-defined big bright structures appear (bright). The distance between two succes-

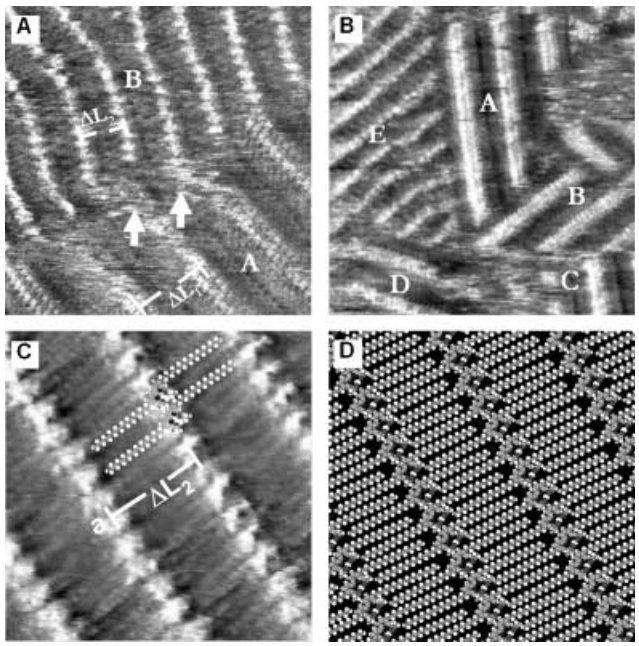

Figure 6. A) STM image showing a monolayer of **2** physisorbed at the liquid/solid interface after addition of $Pd(OAc)_2$. Domain A, uncomplexed. Domain B, complexed. $\Delta L_1 = 47.5 \pm 1.1$ Å and $\Delta L_2 = 35.1 \pm 1.3$ Å. The image size is 21.5×21.5 nm^2; $I_{set} = 0.6$ nA, $V_{set} = -0.418$ V. B) STM image showing uncomplexed domains A, B, C, and D, while domain E is complexed. The image size is 34.6×34.6 nm^2; $I_{set} = 1.2$ nA, $V_{set} = -0.366$ V. C) Two complexed molecular structures are superimposed for clarity. The image area is 10.2×10.2 nm^2; $I_{set} = 1.2$ nA, $V_{set} = -0.486$ V. D) Tentative molecular model of the monolayer where $a = 9.4 \pm 0.1$ Å and $\Delta L_2 = 35.1 \pm 1.3$ Å.

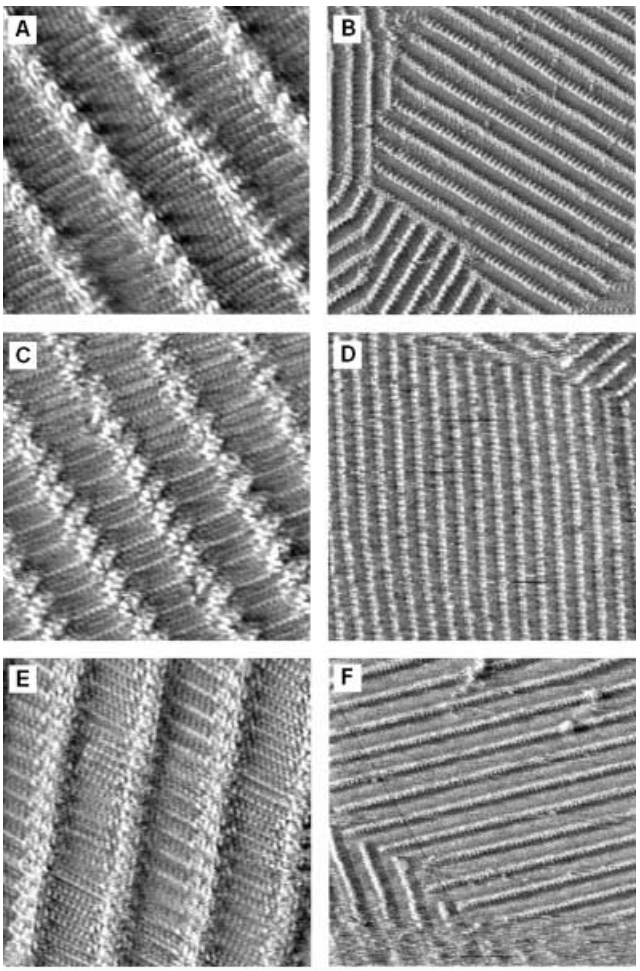

Figure 7. STM images of monolayers of **2** complexed with: (A, B) $PdCl_2$: A) The image area is 11.2×11.3 nm^2; $I_{set} = 1.2$ nA, $V_{set} = -0.142$ V. B) The image area is 50.0×50.0 nm^2; $I_{set} = 1.4$ nA, $V_{set} = -0.160$ V. (C, D) $Cu(OAc)_2$: C) The image area is 12.9×12.9 nm^2; $I_{set} = 0.8$ nA, $V_{set} = -0.450$ V. D) The image area is 50.0×50.0 nm^2; $I_{set} = 0.8$ nA, $V_{set} = -0.472$ V. (E, F) $CuCl_2$: E) The image area is 13.1×13.1 nm^2; $I_{set} = 1.0$ nA, $V_{set} = -0.460$ V. F) The image area is 50.0×50.0 nm^2; $I_{set} = 0.8$ nA, $V_{set} = -0.440$ V.

sive bright structures measured along the lamella axis (a) is 9.4 ± 0.1 Å, which is significantly larger than the distance of 6.9 ± 0.3 Å between bipyridine moieties before the addition of $Pd(OAc)_2$. A change in the packing pattern of the aliphatic chains occurs too, and the chains appear to be interdigitated. The data suggest that one bipyridine unit complexes to each metal complex. This can be explained as follows: the distance between the neighboring molecules increases to 9.4 Å in order to accommodate the $Pd(OAc)_2$ moieties, causing the aliphatic chains to interdigitate in order to reduce the free space in the monolayer, as is revealed by the large decrease in distance between adjacent rows of bipyridine units ($\Delta L_2 = 35.1 \pm 1.3$ Å). It must be noted that the orientation of the aliphatic chains with respect to the lamellar axis changes from $49 \pm 2°$ to $87 \pm 2°$ after addition of $Pd(OAc)_2$. To further clarify the packing pattern, two complexed molecules have been superimposed on the STM image. A molecular model of the observed monolayer packing is shown in Figure 6D.

Furthermore, in situ complexation of **2** with various complexed metal ions such as $PdCl_2$, $Cu(OAc)_2$, and $CuCl_2$ was successfully accomplished. Figure 7A and Figure 7B are STM images of $[Pd(Cl)_2(C19bipyC19)]$ monolayers. The STM images reveal a similar pattern as found for $[Pd(OAc)_2(C19bipyC19)]$ monolayers, with the same unit cell parameters. Figure 6C and Figure 6D show characteristic STM images of $[Cu(OAc)_2(C19bipyC19)]$ monolayers, while Figure 7E and Figure 7F show the corresponding images for $[Cu(Cl)_2(C19bipyC19)]$. Again, the unit cell parameters are not significantly changed. This is quite remarkable given that the nature of the counterion is also different. This robustness in the complexation pattern formed is promising for future complexation experiments, allowing fine-tuning of the complexation properties by using different transition metals. In the case of the in situ addition of the metal complex, the new packing is thought to arise following desorption and readsorption of the molecules in close proximity to the surface.

To accurately compare the behavior of **3** with that of **2** at the liquid/solid interface, complexation of the former with $Pd(OAc)_2$ was also investigated. A spontaneous change in the packing was observed, as depicted in Figure 8A. The molecules are packed in a lamellar-type structure, in which the alkyl chains are interdigitated; two arrows indicate a lamella. Figure 8B also shows an STM image of the complexed monolayer of **3**. The intermolecular distance between neighboring molecules along the lamella is 9.2 ± 0.5 Å. This

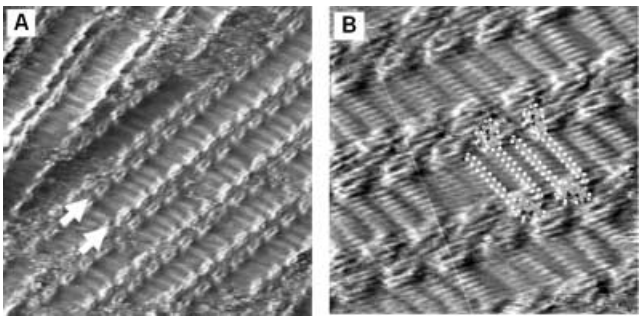

Figure 8. A) Large scale STM image of a monolayer of **3** after the addition of $Pd(OAc)_2$. Only one type of packing is observed, in which the alkyl chains are interdigitated. The image area is 24.1×24.1 nm^2; $I_{set} = 1.3$ nA, $V_{set} = -0.5$ V. B) STM image of a complexed monolayer of **3**. The alkyl chains are clearly interdigitated. The molecular structures of four complexes are superimposed on the image. The image area is 10.8×10.8 nm^2, $I_{set} = 1.2$ nA, $V_{set} = -0.6$ V.

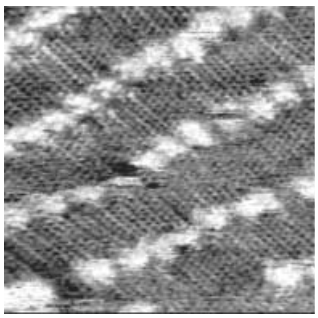

Figure 9. STM image showing a monolayer of **2** physisorbed at the air/solid interface after addition of a solution of $Pd(OAc)_2$ in 1-heptanol and drying for two days under ambient conditions. The image area is 10.2×10.2 nm^2; $I_{set} = 1.00$ nA, $V_{set} = -0.498$ V.

value is identical (within experimental error) to that observed for the complexed monolayer of **2**.[51] Remarkably, after complexation, no different packings are observed; all domains show the same packing. Addition of the metal salts and consequent complexation leads to the formation of a unique 2D pattern.

To exploit the complexed monolayer as a template for building nanostructures, stability of the formed template in air would be a necessity. To assess this stability, a solution of **2** in 1-heptanol was applied to a graphite surface and left to dry under ambient conditions. Following this procedure, STM images similar to those obtained at the liquid/solid interface could be obtained. This does not prove that monolayer films were formed, although locally this is possible. More probably, the STM tip penetrates the deposited material and only the layer in contact with the graphite support is imaged. The observed monolayer was submolecularly resolved, and the packing parameters of the monolayer did not differ from those obtained at the liquid/solid interface. A drop of a $Pd(OAc)_2$ solution in 1-heptanol was then applied on top of the dry layer, and again left to dry under ambient conditions for two days. It seems probable that the formation of the complexed layer involves desorption of the non-complexed molecules and readsorption of the complexed ones, driven by changes in the concentration gradient of complexed and non-complexed molecules in the supernatant solution.[52] Figure 9 shows an image of the complexed monolayer acquired by STM. The image shows similar features to those obtained at the liquid/solid interface.

It is also possible to induce decomplexation at the liquid/solid interface and to restore the metal-free monolayer. This can be achieved, for example, by adding dibromomaleic acid in situ. Addition of dibromomaleic acid leads to a change in the packing pattern of the monolayer. The interdigitated packing pattern of the complexed monolayer is changed to the non-interdigitated one, characteristic of a non-complexed monolayer, indicating the in situ decomplexation of the monolayer by the dibromomaleic acid.

Conclusion

It has been shown that alkylated 2,2′-bipyridines can be used as complexation scaffolds for metal complexes, both at the liquid/solid and liquid/air interfaces. The intermolecular distance within the non-complexed monolayer is of crucial importance in determining whether or not complexation can occur. If the intermolecular distance is too small, as in the case of the urea derivative, no complexation is observed. This is thought to be due to insufficient space between the adsorbed molecules to allow for the accommodation of the metal ions on the surface — due to the stability of the hydrogen-bonded array — or to the desorption of complexed molecules. Addition of a metal complex, either ex situ or in situ, to both symmetric alkylated and asymmetric alkylated bipyridine derivatives leads to complexation. Complexations with different metal ions led to the formation of an identical 2D ordering.

The long-term goal of these experiments is to form stable templates, and then to use such templates for the assembly of other molecules or nanostructures in the third dimension. The stability of such templates in air is a requisite. As a demonstration of such stability, STM investigation of monolayers of **2** before and after evaporation of the solvent revealed identical monolayers. Addition of complexed metal ions led to the formation of complexed monolayers, which were also found to be stable over a period of days. Thus, these potential templates show sufficient stability such that their use in building 3D nanostructures might indeed be possible.To exploit the templating effect, it will be essential to exchange the ligands of the metal complex that are pointing into the supernatant solution with ligands bearing a functional group. Therefore, it will be necessary to test and investigate different complexes with different bonding strengths with respect to the bipyridine molecules or other methods of changing the ligands.

Experimental Section

Materials and methods: All solvents were dried according to standard procedures. Starting materials were purchased from Aldrich or Acros. ^{1}H NMR spectra were recorded on a Varian VXR-300 spectrometer (at

300 MHz) with samples in $CDCl_3$ or [D_6]DMSO; chemical shifts are given in ppm relative to $CDCl_3$ (δ = 7.26 ppm) or DMSO (δ = 2.50 ppm). ^{13}C NMR spectra were recorded on a Varian VXR-300 spectrometer (at 75.48 MHz) with samples in $CDCl_3$ or [D_6]DMSO; chemical shifts are given relative to $CDCl_3$ (δ = 77 ppm) or DMSO (δ = 39.5 ppm) The splitting patterns in the ^{1}H NMR spectra are designated as follows: s (singlet), d (doublet), dd (double doublet), t (triplet), m (multiplet), br (broad). Melting points were measured on a Stuart Scientific SMP1 apparatus. Infrared spectra were recorded on a Nexus FTIR spectrometer. HRMS was performed on a JEOL JMS 600H spectrometer in EI$^+$ ionization mode. Elemental analyses were carried out in the Microanalytical Department of the Stratingh Institute, University of Groningen (The Netherlands).

Synthesis of bromopropanol THP ether: 3,4-2*H*-Dihydropyran (12 mL; excess) was added to a solution of bromopropanol (15 g, 0.11 mol) in CH_2Cl_2 (60 mL) at 0 °C. The mixture was stirred for 4 h at room temperature. It was then washed with water (100 mL), and the aqueous layer was extracted wih CH_2Cl_2 (2×100 mL). The combined organic layers were washed with brine, dried ($MgSO_4$), and concentrated in vacuo. The brown-yellow oil was purified by column chromatography (silica; hexane/diethyl ether (10%)) to yield a colorless oil. Yield 18.9 g (0.085 mol, 80%); ^{1}H NMR (300 MHz, $CDCl_3$): δ = 4.51 (t, J = 2.9 Hz, 1H), 3.82–3.74 (m, 2H), 3.47–3.39 (m, 4H), 2.05 (quintet, ^1J = 6.2 Hz, ^3J = 12.5 Hz, 2H), 1.7–1.4 ppm (m, 6H).

Synthesis of 5-methyl,5′-((tetrahydropyranyloxy)butyl)-2,2′-bipyridine: A solution of LDA (30 mmol) was freshly prepared from diisopropylamine (4.6 mL) and *n*BuLi (19 mL, 1.6 M in hexanes) in THF (10 mL) at −80 °C. A solution of 5,5′-dimethyl-2,2′-bipyridine (5.0 g, 27 mmol) in THF (150 mL) was then added at the same temperature. The reaction mixture, which immediately turned black, was stirred for 2 h at −80 °C. It was then allowed to warm to room temperature, whereupon a solution of bromopropanol THP ether (7.8 g, 35 mmol) in THF (40 mL) was added. The mixture was stirred at rt for 100 h, then quenched with MeOH and poured into ice-water (300 mL). The resulting mixture was extracted with Et_2O (4×200 mL), and the combined organic layers were dried (Na_2SO_4) and concentrated in vacuo.

The product was further purified by column chromatography (silica; elution with 2% MeOH in CH_2Cl_2) to yield the pure material as an orange-brown oil. Yield 7.8 g (24 mmol, 90%); ^{1}H NMR (300 MHz, $CDCl_3$): δ = 8.46 (s, 2H), 8.22 (dd, J = 3.9 Hz, 2H), 7.62–7.55 (m, 2H), 4.55 (s, 1H), 3.82–3.72 (m, 2H), 3.49–3.41 (m, 2H), 2.67 (t, J = 6.9 Hz, 2H), 2.35 (s, 3H), 1.77–1.50 ppm (m, 12H).

Synthesis of 5,5′-bis((tetrahydropyranyloxy)butyl)-2,2′-bipyridine: The same procedure was followed as for the synthesis of the monosubstituted derivative. A solution of the monosubstituted derivative (7.8 g, 24 mmol) in THF (150 mL) was added to freshly prepared LDA solution (30 mmol). Subsequently, a solution of the bromopropanol THP ether (9.0 g, 0.04 mol) was added. After work-up, the title disubstituted bipyridine was obtained as a brown oil. Yield: 9.6 g (0.021 mol, 88%); ^{1}H NMR (300 MHz, $CDCl_3$): δ = 8.46 (s, 2H), 8.23 (d, J = 8.1 Hz, 2H), 7.59 (d, J = 8.3 Hz, 2H), 4.54 (s, 2H), 3.86–3.70 (m, 4H), 3.53–3.33 (m, 4H), 2.67 (t, J = 6.6 Hz, 4H), 1.81–1.50 ppm (m, 20H); ^{13}C NMR (300 MHz, $CDCl_3$): δ = 152.5, 147.7, 136.1, 135.3, 118.9, 65.6, 61.4, 60.8, 31.4, 29.1, 27.7, 26.3, 24.0, 18.1 ppm.

Synthesis of 5,5′-bis(hydroxybutyl)-2,2′-bipyridine: The protected bipyridine (5.0 g, 10.7 mmol) was dissolved in EtOH (120 mL) and *p*-toluenesulfonic acid (0.5 g) was added. The mixture was refluxed for 24 h, then neutralized with triethylamine. The ethanol was evaporated and the crude product was redissolved in $CHCl_3$. This solution was filtered through neutral aluminum oxide, the filtrate was concentrated to a viscous oil, and this was suspended in toluene. The product separated as a white solid upon sonication.

Yield: 1.1 g (3.7 mmol, 35%); ^{1}H NMR (300 MHz, $CDCl_3$): δ = 8.50 (s, 2H), 8.26 (d, J = 8.3 Hz, 2H), 7.64 (d, J = 8.3 Hz, 2H), 3.66 (t, J = 6.4 Hz, 4H), 2.69 (t, J = 6.6 Hz, 4H), 1.79–1.58 ppm (m, 8H); ^{13}C NMR (300 MHz, $CDCl_3$): δ = 152.3, 147.4, 136.1, 135.3, 119.3, 60.9, 31.0, 30.6, 25.7 ppm; MS: m/z: 300, 255; HRMS: calcd for $C_{18}H_{24}N_2O_2$ 300.18376; found 300.18438.

Synthesis of 5,5′-bis(bromobutyl)-2,2′-bipyridine: Concentrated H_2SO_4 (0.25 mL, 4 mmol) was added to a solution of the diol (0.5 g, 1.8 mmol) in 48% aqueous HBr (5 mL). The reaction mixture was refluxed for 12 h, then diluted with ice-water (80 mL), and neutralized with aqueous Na_2CO_3 solution (20 mL). The yellow mass that was liberated was extracted with $CHCl_3$ (5×50 mL) and the combined organic phases were dried (Na_2SO_4) and purified by column chromatography (CH_2Cl_2/toluene, 2:8). Evaporation of the solvents gave the dibromide as a white solid. Yield: 0.6 g (1.4 mmol, 78%); ^{1}H NMR (300 MHz, $CDCl_3$): δ = 8.48 (s, 2H), 8.26 (d, J = 8.0 Hz, 2H), 7.62 (d, J = 8.1 Hz, 2H), 3.42 (t, J = 7.1 Hz, 4H), 2.68 (t, J = 6.9 Hz, 4H), 2.67 (t, J = 6.9 Hz, 2H), 2.02–1.66 ppm (m, 8H); ^{13}C NMR (300 MHz, $CDCl_3$): δ = 147.8, 135.3, 130.5, 127.1, 119.1, 34.6, 30.8, 26.9, 20.0 ppm; MS: m/z: 426, 277; HRMS: calcd for $C_{18}H_{22}N_2Br_2$ 424.01489; found 424.01361.

Synthesis of 5,5′-bis(azidobutyl)-2,2′-bipyridine: NaN_3 (400 mg, 6.2 mmol, 4 equiv.) was added to a solution of the aforementioned 5,5′-bis(bromobutyl)-2,2′-bipyridine (0.6 g, 1.4 mmol) in DMSO (10 mL). The reaction mixture was stirred at 50 °C for 12 h. It was then poured into water (50 mL), and the resulting mixture was extracted with Et_2O (3×50 mL). The combined organic phases were dried (Na_2SO_4) and concentrated *in vacuo* to provide the product as a yellow oil.

Yield: 0.48 g (1.4 mmol, 100%); ^{1}H NMR (300 MHz, $CDCl_3$): δ = 8.49 (s, 2H), 8.29 (d, J = 8.1 Hz, 2H), 7.62 (dd, ^1J = 8.1 Hz, ^2J = 2.2 Hz, 2H), 3.31 (t, J = 6.6 Hz, 4H), 2.71 (t, J = 6.9 Hz, 4H), 1.76–1.66 ppm (m, 8H); ^{13}C NMR (300 MHz, $CDCl_3$): δ = 147.8, 135.3, 130.5, 127.1, 119.1, 49.7, 30.8, 26.9, 20.0 ppm.

Synthesis of 5,5′-bis(aminobutyl)-2,2′-bipyridine: The aforementioned 5,5′-bis(azidobutyl)-2,2′-bipyridine (0.5 g, 1.4 mmol) was dissolved in EtOH (20 mL), and 10% Pd/C (50 mg) was added. A balloon filled with H_2 gas was attached to the top of the flask, and the mixture was vigorously stirred for 12 h under the H_2 atmosphere. The mixture was subsequently filtered through Celite and the filtrate was dried (Na_2SO_4) and concentrated *in vacuo*.

The product was further purified by acid-base extraction to give a yellow oil that solidified on standing. Yield: 0.41 g (1.4 mmol, 100%); ^{1}H NMR (300 MHz, $CDCl_3$ + [D_6]DMSO): δ = 8.19 (s, 2H), 7.96 (d, J = 8.1 Hz, 2H), 7.35 (dd, ^1J = 8.1 Hz, ^2J = 2.2 Hz, 2H), 2.45–2.29 (m, 8H, CH_2NH_2 + CH_2Pyr), 1.39 (t, J = 6.6 Hz, 4H), 1.24 ppm (t, J = 7.0 Hz, 4H); ^{13}C NMR (300 MHz, $CDCl_3$): δ = 146.6, 134.1, 130.5, 127.1, 117.7, 39.2, 30.5, 29.9, 25.7 ppm.

Synthesis of 5,5′-bis(dodecylureidobutyl)-2,2′-bipyridine: 5,5′-Bis(aminobutyl)-2,2′-bipyridine (0.3 g, 1.1 mmol) was added to toluene (30 mL). The mixture was heated to reflux, until it became a smooth and slightly transparent suspension. At this point, a solution of dodecyl isocyanate (800 mg, 3.8 mmol, >3 equiv) in toluene (5 mL) was added. Almost immediately, a white solid started to precipitate. The mixture was stirred while slowly (over a period of 1 h) cooling down to room temperature. The white precipitate was collected by suction filtration, and further purified by resuspending it, on the filter, in acetone, methanol, and diethyl ether, respectively, followed by suction. The product was dried at 80 °C, 3 mmHg. Yield: 0.2 g (0.3 mmol, 30%); off-white solid; m.p. 220 °C (decomp); ^{1}H NMR (300 MHz, [D]TFA/[D_6]DMSO): δ = 8.54 (s, 2H), 8.24 (d, J = 8.1 Hz, 2H), 8.05 (d, J = 8.1 Hz, 2H), 3.09 (t, J = 6.6 Hz, 4H), 2.99 (t, J = 7.0 Hz, 4H), 2.70 (t, J = 7.0 Hz, 4H), 1.59 (m, 4H), 1.46 (m, 4H), 1.30–0.99 (m, 40H), 0.70 ppm (t, J = 6.6 Hz, 6H); ^{13}C NMR (300 MHz, [D_6]DMSO/TFA): δ = 145.5, 139.6, 123.7, 121.9, 116.1, 31.4, 31.1, 29.8, 29.4, 28.8, 28.5, 28.4, 27.3, 26.8, 26.2, 21.7, 13.4 ppm; IR (KBr): $\tilde{\nu}$ = 3350, 2956, 1625, 1575, 1466 cm^{-1}; MS: m/z = 721.7; elemental analysis calcd for $C_{44}H_{76}N_6O_2$: C 73.29, H 10.62; found: C 72.98, H 10.43.

Synthesis of 5′-methyl-5-nonadecyl-2,2′-bipyridine: A mixture of diisopropylamine (800 μL, 580 mg, 5.7 mmol) and *n*BuLi (1.6 M in hexanes; 3.5 mL, 5.6 mmol) in THF (10 mL) was first stirred at −78 °C for 15 min. A solution of 5,5′-dimethyl-2,2′-bipyridine (1.0 g, 5.45 mmol) in THF (50 mL) was then added from a dropping funnel over a period of 30 min. The reaction mixture was stirred for an additional 2 h, while the temperature was slowly raised to 0 °C. A solution of octadecyl bromide (2.0 g, 6 mmol, 1.1 equiv.) in THF (5 mL) was then added by means of a syringe. The mixture was stirred for 48 h at room temperature, and then ice was added. The product was extracted with Et_2O, and the combined extracts were washed with aqueous $NaHCO_3$ solution and water, and then concentrated. The residue was recrystallized twice from $CHCl_3$. Yield: 1.3 g

(3.0 mmol, 55%); white powder; m.p. 74–75°C; ^{1}H NMR (300 MHz, $CDCl_3$): δ = 8.43 (s, 2H), 8.20 (d, J = 8.0 Hz, 1H), 8.19 (d, J = 8.0 Hz, 1H), 7.55 (d, J = 8.0 Hz, 2H), 2.59 (t, J = 7.8 Hz, 2H), 2.33 (s, 3H), 1.57 (m, 2H), 1.19 (m, 32H), 0.82 ppm (t, J = 6.8 Hz, 3H); ^{13}C NMR (300 MHz, $CDCl_3$): δ = 154.0, 149.6, 149.3, 138.0, 137.5, 136.8, 133.1, 120.5, 120.4, 32.9, 32.0, 31.5, 29.8, 29.4, 29.2, 22.7, 14.1 ppm; MS: m/z: 436, 407, 393, 379, 365, 351, 337, 323, 309, 295, 281, 267, 253, 239, 211, 197, 184; elemental analysis calcd for $C_{30}H_{48}N_2$: C 82.51, H 11.08, N 6.41; found: C 82.33, H 11.73, N 6.30.

Synthesis of 5,5′-bis(nonadecyl)-2,2′-bipyridine: The procedure described above was repeated, but with diisopropylamine (350 μL, 2.4 mmol) and *n*BuLi (1.5 mL, 2.4 mmol) in THF (10 mL), 5′-methyl-5-nonadecyl-2,2′-bipyridine (1 g, 2.35 mmol) in THF (50 mL), and octadecyl bromide (850 mg, 2.55 mmol). Upon addition of ice in the work-up, the product precipitated. It was collected by suction filtration and recrystallized twice from $CHCl_3$ to provide a white powder.

Yield: 820 mg (1.2 mmol, 40%); m.p. 99–100°C; ^{1}H NMR (300 MHz, $CDCl_3$): δ = 8.46 (s, 2H), 8.23 (d, J = 8.0 Hz, 2H), 7.59 (dd, ^1J = 8.1 Hz, ^3J = 1.8 Hz, 2H), 2.63 (t, J = 7.8 Hz, 2H), 1.61 (m, 4H), 1.23 (m, 64H), 0.82 ppm (t, J = 6.8 Hz, 6H); ^{13}C NMR (300 MHz, $CDCl_3$): δ = 156.3, 149.3, 138.0, 136.8, 120.5, 32.9, 32.0, 31.2, 29.8, 29.5, 29.4, 29.2, 22.8, 14.2 ppm; MS: m/z: 688, 449, 321; elemental analysis calcd for $C_{48}H_{84}N_2$: C 83.65, H 12.28, N 4.06; found: C 82.90, H 12.26, N 4.36.

STM: Prior to imaging, all compounds to be investigated were dissolved in 1-octanol or 1-phenyloctane, and a drop of this solution was applied to a freshly cleaved surface of highly oriented pyrolytic graphite (HOPG). The STM images were acquired in the variable current mode (constant height) under ambient conditions with the tip immersed in the liquid. In the acquired STM images, white corresponds to the highest and black to the lowest measured tunneling current. STM experiments were performed using a Discoverer scanning tunneling microscope (Topometrix Inc., Santa Barbara, CA) along with an external pulse/function generator (Model HP 8111A), with negative sample bias. Tips were electrochemically etched from Pt/Ir wire (80%/20%, diameter 0.2 mm) in a 2N KOH/6N NaCN solution in water. All complexation reactions were performed in situ, unless stated otherwise. Therefore, a drop of the concentrated solution of the metal complex (in 1-octanol or 1-phenyloctane) was added to the sample. For solubility reasons, in some reactions a co-solvent was used (see text). These co-solvents were selected such that they had low boiling points and that the metal ions would be known to complex to the bipyridine in the resulting medium.

The experiments were repeated in several sessions using different tips to check for reproducibility and to avoid artefacts. Different settings of the tunneling current and the bias voltage were used, ranging from 0.3 nA to 1.0 nA and −10 mV to −1.5 V, respectively. All STM images are derived from raw data and have not been subjected to any manipulation or image processing.

Acknowledgements

The authors thank the DWTC, through IUAP-V-03, the Institute for the promotion of innovation by Sciences and Technology in Flanders (IWT). ESF SMARTON made the Leuven–Groningen collaboration possible. S.D.F. is a postdoctoral fellow of the Fund for Scientific Research, Flanders. J.v.E. gratefully acknowledges the Royal Academy of the Netherlands for a fellowship. B.V. is an Erasmus student from the University of Groningen, the Netherlands.

[1] *Handbook of Microlithography, Micromachining, and Microfabrication* (Ed.: P. Rai-Choudhury), SPIE Optical Engineering Press, London, **1997**.
[2] Y. Xia, G. M. Whitesides, *Angew. Chem.* **1998**, *110*, 568; *Angew. Chem. Int. Ed.* **1998**, *37*, 550.
[3] R. M. Nyffenegger, R. M. Penner, *Chem. Rev.* **1997**, *97*, 1195.
[4] G.-Y. Liu, S. Xu, Y. Qian, *Acc. Chem. Res.* **2000**, *33*, 457.
[5] W. T. Müller, D. L. Klein, T. Lee, J. Clarke, P. L. McEuen, P. G. Schultz, *Science* **1995**, *268*, 272.
[6] R. Maoz, S. R. Cohen, J. Sagiv, *Adv. Mater.* **1999**, *11*, 55.
[7] J. Zhao, K. Uosaki, *Langmuir* **2001**, *17*, 7784.
[8] J. Zhao, K. Uosaki, *Nano Lett.* **2002**, *2*, 137.
[9] C. B. Gorman, R. L. Carroll, Y. He, F. Tian, R. Fuierer, *Langmuir* **2000**, *16*, 6312.
[10] C. B. Gorman, R. L. Carroll, R. Fuierer, *Langmuir* **2001**, *17*, 6923.
[11] R. D. Piner, J. Zhu, F. Xy, S. Hong, C. A. Mirkin, *Science* **1999**, *283*, 661.
[12] S. Jahromi, J. Dijkstra, E. van der Vegte, B. Mostert, *ChemPhysChem* **2002**, *3*, 693.
[13] B. W. Maynor, S. F. Filocamo, M. W. Grinstaff, J. Liu, *J. Am. Chem. Soc.* **2002**, *124*, 522.
[14] S. Sun, K. S. L. Chong, G. J. Leggett, *J. Am. Chem. Soc.* **2002**, *124*, 2414.
[15] *Comprehensive Supramolecular Chemistry* (Eds.: J. L. Atwood, J. E. D. Davies, D. D. MacNicol, F. Vögtle), Pergamon, New York, **1996**.
[16] M. S. Boeckl, T. Baas, A. Fujita, K. O. Hwang, A. L. Bramblett, B. D. Ratner, J. W. Rogers, T. Sasaki, *Biopolymers* **1998**, *47*, 185.
[17] G. Koller, S. Surnev, F. P. Netzer, M. N. G. Ramsey, *Surf. Sci.* **2002**, *504*, 1–3, 11.
[18] D. G. Yablon, D. Wintgens, G. W. Flynn, *J. Phys. Chem. B* **2002**, *106*, 21, 5470.
[19] D. Moll, C. Huber, B. Schlegel, D. Pum, U. B. Sleytr, M. Sara, *Proc. Natl. Acad. Sci. USA* **2002**, *99*, 23, 14646.
[20] E. Dujardin, C. Peet, G. Stubbs, J. N. Culver, S. Mann, *Nano Lett.* **2003**, *3*, 3, 413.
[21] W. A. Hayes, C. Shannon, *Langmuir* **1998**, *14*, 5, 1099.
[22] N. Lu, M. Gleiche, J. W. Zheng, S. Lenhert, B. Xu, L. F. Chi, H. Fuchs, *Adv. Mater.* **2002**, *14*, 24, 1812.
[23] A. Ulman, *Chem. Rev.* **1996**, *96*, 1533–1554, and references therein.
[24] P. A. Lewis, Z. J. Donhauser, B. A. Mantooth, R. K. Smith, L. A. Bumm, K. F. Kelly, P. S. Weiss, *Nanotechnology* **2001**, *12*, 231, and references therein.
[25] H. Rapaport, I. Kuzmenko, M. Berfeld, K. Kjaer, J. Als-Nielsen, R. Popovitz-Biro, I. Weissbuch, M. Lahav, L. Leiserowitz, *J. Phys. Chem. B* **2000**, *104*, 1399.
[26] I. Weissbuch, M. Berfeld, W. Bouwman, K. Kjaer, J. Als-Nielsen, M. Lahav, L. Leiserowitz, *J. Am. Chem. Soc.* **1997**, *119*, 933.
[27] A. Semenov, J. P. Spatz, M. Möller, J.-M. Lehn, B. Sell, D. Schubert, C. H. Weidl, U. S. Schubert, *Angew. Chem.* **1999**, *111*, 17, 2701; *Angew. Chem. Int. Ed.* **1999**, *38*, 2547.
[28] U. Ziener, J.-M. Lehn, A. Mourran, M. Möller, *Chem. Eur. J.* **2002**, *8*, 951.
[29] D. P. Funeriu, J.-M. Lehn, K. M. Fromm, D. Fenske, *Chem. Eur. J.* **2000**, *6*, 12, 2103.
[30] B. Hasenknopf, J.-M. Lehn, N. Boumediene, E. Leize, A. Van Dorsselaer, *Angew. Chem.* **1998**, *110*, 23, 3458; *Angew. Chem. Int. Ed.* **1998**, *37*, 23, 3265.
[31] J.-M. Lehn, *Chem. Eur. J.* **2000**, *6*, 12, 2097.
[32] A. Dmitriev, H. Spillman, N. Lin, J. V. Barth, K. Kern, *Angew. Chem.* **2003**, *115*, 2774; *Angew. Chem. Int. Ed.* **2003**, *42*, 23, 2670.
[33] N. Lin, A. Dmitriev, J. Weckesser, J. V. Barth, K. Kern, *Angew. Chem.* **2002**, *114*, 4973; *Angew. Chem. Int. Ed.* **2002**, *41*, 24, 4779.
[34] P. Messina, A. Dmitriev, N. Lin, H. Spillman, M. Abel, J. V. Barth, K. Kern, *J. Am. Chem. Soc.* **2002**, *124*, 47, 14000.
[35] D. G. Kurth, N. Severin, J. P. Rabe, *Angew. Chem.* **2002**, *114*, 3833; *Angew. Chem. Int. Ed.* **2002**, *41*, 3681.
[36] S. Hoeppener, J. Wonnemann, L. Chi, G. Erker, H. Fuchs, *ChemPhysChem.* **2003**, *4*, 490.
[37] S. Hoeppener, L. Chi, H. Fuchs, *ChemPhysChem.* **2003**, *4*, 494.
[38] M. M. S. Abdel-Mottaleb, N. Schuurmans, S. De Feyter, J. van Esch, B. L. Feringa, F. C. De Schryver, *Chem. Commun.* **2002**, 1894.
[39] M. Fujita, *Struct. Bonding (Berlin, Ger.)*, **2000**, 96, 177.
[40] R. Ziessel, J. Suggert, M. T. Youinou, *J. Org. Chem.* **1996**, *61*, 6535.
[41] S. Leininger, B. Olenyuk, P. J. Stang, *Chem. Rev.* **2000**, *100*, 853.
[42] M. Fujita, *Chem. Soc. Rev.* **1998**, *27*, 417.
[43] D. Philip, J. F. Stoddart, *Angew. Chem.* **1996**, *108*, 1242; *Angew. Chem. Int. Ed.* **1996**, *35*, 1154.
[44] M. J. Zaworotko, *Angew. Chem.* **2000**, *112*, 17, 3180; *Angew. Chem. Int. Ed.* **2000**, *39*, 3052.

[45] S. De Feyter, K. Grim, J. van Esch, R. M. Kellogg, B. L. Feringa, F. C. De Schryver, *J. Phys. Chem. B* **1998**, *102*, 8981.
[46] A. Gesquière, M. M. S. Abdel-Mottaleb, S. De Feyter, F. C. De Schryver, F. Schoonbeek, J. van Esch, R. M. Kellogg, B. L. Feringa, A. Calderone, R. Lazzaroni, J. L. Brédas, *Langmuir* **2000**, *16*, 10385.
[47] S. De Feyter, M. Larsson, A. Gesquière, H. Verheyen, F. Louwet, B. Groenendaal, J. van Esch, B. L. Feringa, F. C. De Schryver, *ChemPhysChem* **2002**, *3*, 966.
[48] S. De Feyter, M. Larsson, N. Schuurmans, B. Verkuijl, G. Zoriniants, A. Gesquière, M. M. Abdel-Mottaleb, J. van Esch, B. L. Feringa, J. van Stam, F. De Schryver, *Chem. Eur. J.* **2003**, *9*, 5, 1198.
[49] F. S. Schoonbeek, J. H. van Esch, B. Wegewijs, D. B. A. Rep, M. P. De Haas, T. M. Klapwijk, R. M. Kellogg, B. L. Feringa, *Angew. Chem.* **1999**, *111*, 10, 1486; *Angew. Chem. Int. Ed.* **1999**, *38*, 1393.
[50] In solution, it is known that the transoid conformation is thermodynamically favored: a) S. T. Howard, *J. Am. Chem. Soc.* **1996**, *118*, 10269; b) L. A. Cuccia, J.-M. Lehn, J. C. Homo, M. Schmutz, *Angew. Chem.* **2000**, *112*, 1, 239; *Angew. Chem. Int. Ed.* **2000**, *39*, 1, 233.
[51] In this image, the alkyl chains appear as broad bands aligned in a row perpendicular to the lamellar axis. This contrast is thought to be due to scanner drift. This effect was also observed for the bipyridine moieties and the underlying graphite lattice.
[52] R. Heinz, A. Stabel, J. P. Rabe, G. Wegner, F. C. De Schryver, D. Corens, W. Dehaen, C. Süling, *Angew. Chem.* **1994**, *106*, 2154; *Angew. Chem. Int. Ed. Engl.* **1994**, *33*, 2080.

Received: August 1, 2003 [F5424]